Supporting Information

Near-Field Imaging of Infrared Nanoantenna Modes Under Oblique Illumination

Shingo Usui,[†] Shuta Kitade,[‡] Ikki Morichika,[‡] Kensuke Kohmura,[†] Fumiya Kusa,[†,‡] and Satoshi Ashihara[*,†,‡]

[†]Department of Applied Physics, Tokyo University of Agriculture and Technology, 2-24-16, Nakacho, Koganei, Tokyo, 184-8588, Japan

[‡]Institute of Industrial Science, The University of Tokyo, 4-6-1, Komaba, Meguro-ku, Tokyo, 153-8505, Japan

*ashihara@iis.u-tokyo.ac.jp

■ EXPERIMENTAL SETUP FOR S-SNOM

Our developed s-SNOM shown in Fig. S1 is based on a commercial AFM (Hitachi High-Tech Science, NanoNavi II-TE100SPM) operating in the tapping-mode (frequency Ω of ~400 kHz). The light source is a linearly-polarized CO_2 laser at the wavelength of 10.6 μm (Access Laser Company, L3SL). The beam diameter is expanded from 2.5 mm to 12.5 mm and the polarization direction is adjusted with a half-wave plate. The laser beam is directed toward the Michelson interferometer with a ZnSe beam splitter. One beam is focused by an off-axis parabolic mirror (NA = 0.5) onto the sample and the uncoated Si-tip (apex radius of 20 nm), with the focal spot size of 30 μm in diameter. Here the laser beam is incident onto the sample plane with an incidence angle of 60°. The light scattered at the Si-tip is collected by the same parabolic mirror, recombined with the other beam which is reflected at a mirror attached on a piezoelectric actuator (Physik Instrumente GmbH & Co., P-841.10), and directed toward a HgCdTe detector (Teledyne Judson Technologies, J19D12-M204-R250U-60-WE). The polarizer is used to select the polarization component to be detected. In order to suppress the strong background scattering noise, the signal modulated at a harmonics of Ω is detected using a lock-in amplifier. Being mixed with the stronger reference light, the backscattered signal is amplified. Furthermore, amplitude- and phase resolved measurement is achieved through the interferometric homodyne detection. The spatial resolution of the s-SNOM measurement is well below 60 nm, evaluated from a measurement on a test Cr pattern.

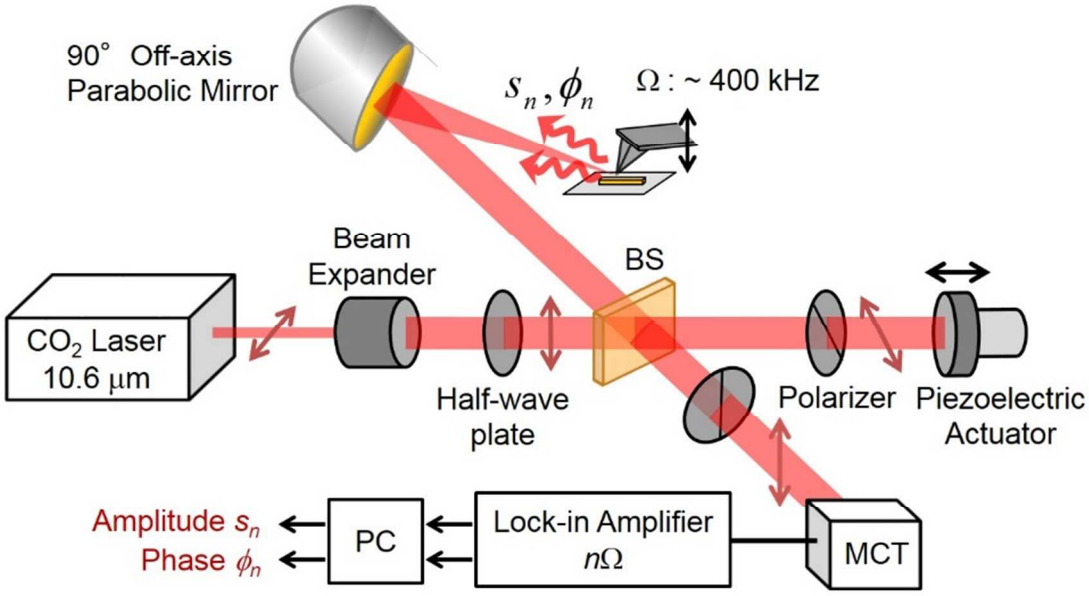

Figure S1. Experimental setup for the IR s-SNOM. The light scattered from the Si-tip is collected by the parabolic mirror, recombined with the reference beam, and directed toward the HgCdTe (MCT) detector. The signal modulated at a harmonics of the AFM tapping frequency Ω is detected using a lock-in amplifier The amplitude s_n and the phase ϕ_n of the scattered light is measured by the interferometric homodyne detection.

■ ANALYSES ON THE TOPOGRAPHIC IMAGES

Figure S2 shows (a) the AFM topographic image for the Au nanorod of L = 2.8 μm (the same image as that shown in Fig.3(a)) and (b) the topographic line profile taken along the longer axis evaluated at the middle of the nanorod (a black solid line). The nanorod width evaluated from the topographic line profile along the shorter axis at each x-position is also shown in Fig. S2 (b) as open circles. Figure S3 shows the corresponding data for the Au nanorod of L = 5.8 μm.

The height of the nanorod is 63 ± 10 nm and 73 ± 15 nm for the nanorod of L = 2.8 μm and 5.8 μm, respectively. The width of the nanorod is evaluated to be 192 ± 20 nm and 203 ± 17 nm for the nanorod of L = 2.8 μm and 5.8 μm, respectively. The observed fluctuations in height and those in width, both of which are about 20 nm, would originate from polycrystalline grain structures of the evaporated Au films. The fluctuations are rather random, and there is no noticeable asymmetry in the topographic profiles in the direction along the nanorod longer axis.

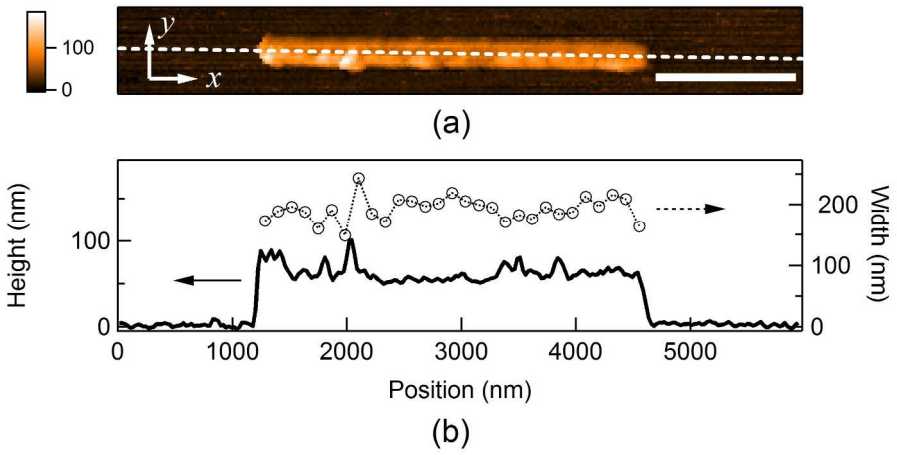

Figure S2. (a) The AFM topographic image for the Au nanorod of L = 2.8 μm. (b) The topographic line profile, taken along the longer axis evaluated at the middle of the nanorod (a white dashed line in (a)), is shown as a black solid line for the left axis. The nanorod width evaluated at each x-position is shown as an open circle for the right axis.

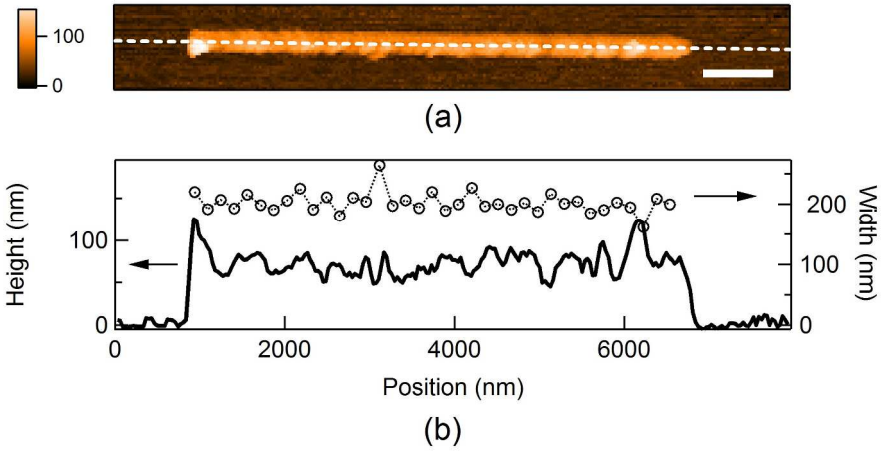

Figure S3. (a) The AFM topographic image for the Au nanorod of L = 5.8 μm. (b) The topographic line profile, taken along the longer axis evaluated at the middle of the nanorod (a white dashed line in (a)), is shown as a black solid line for the left axis. The nanorod width evaluated at each x-position is shown as an open circle for the right axis.

■ ELECTRIC FIELDS ALONG THE NANOROD LONGER AXES

We present the results of the FDTD numerical simulations on the near-field distributions of *x*-component (along the nanorod longer axes) for optical excitation at the wavelength of 10.6 μm. Figures S4 and S5 display the results for the nanorod length of L = 2.8 and 5.8 μm, respectively. Each of the figures displays (a, e) the amplitude images (*x*-component), (b, f) their line profiles, (c, g) the phase images, and (d, h) their line profiles, upon optical excitation (a-d) at normal incidence and (e-h) at oblique incidence (incidence angle of 60°). The line profiles are taken along the nanorod longer axis at the middle of the nanorod. We can see that the asymmetries found for *x*-components are similar to the ones found for *z*-components shown in Figs. 6 and 7.

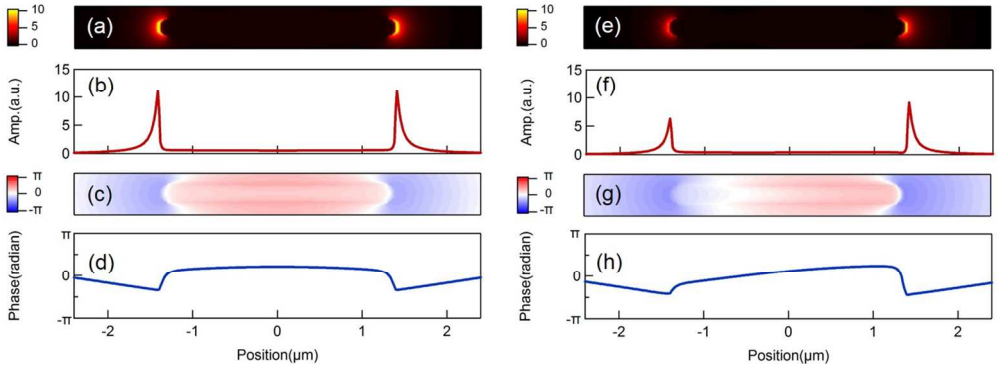

Figure S4. Simulated near-field distributions (*x*-component) for the Au nanorod of L = 2.8 μm (a-d) under the normal incidence and (e-h) under the oblique incidence with an incidence angle of 60°: (a, e) the amplitude images, (b, f) their line profiles, (c, g) the phase images, and (d, h) their line profiles.

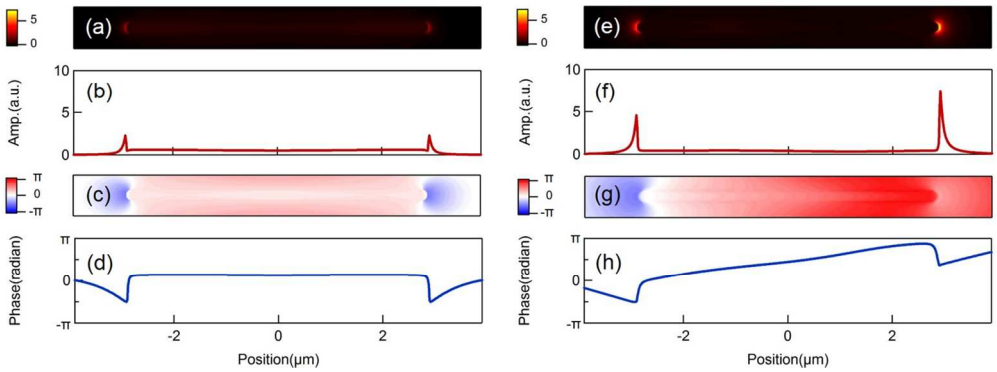

Figure S5. Simulated near-field distributions (*x*-component) for the Au nanorod of L = 5.8 μm (a-d) under the normal incidence and (e-h) under the oblique incidence with an incidence angle of 60°: (a, e) the amplitude images, (b, f) their line profiles, (c, g) the phase images, and (d, h) their line profiles.